AD NUMBER
AD085782
LIMITATION CHANGES
TO: **Approved for public release; distribution is unlimited.**
FROM: **Distribution authorized to U.S. Gov't. agencies and their contractors; Administrative/Operational Use; NOV 1955. Other requests shall be referred to Army Ballistic Research Laboratory, Aberdeen Proving Ground, MD 21005.**
AUTHORITY
usabrl ltr 22 apr 1981

BRL

FC

MEMORANDUM REPORT No. 947

NOVEMBER 1955

Effect Of A Hemispherical Base On The Aerodynamic Characteristics Of Shell

RALPH E. DEITRICK

DEPARTMENT OF THE ARMY PROJECT No. 5B03-03-001
ORDNANCE RESEARCH AND DEVELOPMENT PROJECT No. TB3-0108

BALLISTIC RESEARCH LABORATORIES

ABERDEEN PROVING GROUND, MARYLAND

B A L L I S T I C R E S E A R C H L A B O R A T O R I E S

MEMORANDUM REPORT NO. 947

NOVEMBER 1955

EFFECT OF A HEMISPHERICAL BASE ON THE AERODYNAMIC CHARACTERISTICS OF SHELL

Ralph E. Deitrick

Department of the Army Project No. 5B03-03-001
Ordnance Research and Development Project No. TB3-0108

A B E R D E E N P R O V I N G G R O U N D, M A R Y L A N D

TABLE OF CONTENTS

B A L L I S T I C R E S E A R C H L A B O R A T O R I E S

MEMORANDUM REPORT NO. 947

REDeitrick/bdb
Aberdeen Proving Ground, Md.
November 1955

EFFECT OF A HEMISPHERICAL BASE ON THE AERODYNAMIC CHARACTERISTICS OF SHELL

ABSTRACT

The addition of a hemispherical base to a square based model produces marked dynamic instability. A comparison of the aerodynamic characteristics of square and hemispherical based models is given. Estimates of the damping and Magnus forces of the hemispherical based model are obtained. The reason for the instability is quite clear although the mechanism which produces this result seems quite complex.

TABLE OF SYMBOLS

c.m.		Center of mass of projectile
$C.P._N$		Center of pressure of normal force
$C.P._{\Delta K_i}$		Center of pressure of the increment of force between the square and hemispherical based models
d		Diameter of projectile
K_D		Drag force coefficient
K_{D_o}	=	K_D when $\delta = 0$
$K_{D_{\delta^2}}$	=	$\left(\frac{\partial K_D}{\partial \delta^2}\right)_{\delta = 0}$
K_L		Lift force coefficient
K_N		Normal force coefficient
K_M		Overturning moment coefficient
K_F		Magnus force coefficient
K_T		Magnus moment coefficient
K_S		Damping force coefficient
K_H		Damping moment coefficient
K_A		Spin deceleration moment coefficient
K_i^*		Square based model coefficient corrected to a location corresponding to the c.m. of the equivalent length hemispherical based model.
$\hat{K}_i$		Estimated coefficient of the hemispherical based model
k_1		Axial radius of gyration
k_2		Transverse radius of gyration
K_1		Amplitude of fast rate of yawing motion
K_2		Amplitude of slow rate of yawing motion
m		Mass of projectile
M		Mach number
s	=	$\frac{A^2 \omega_1^2}{4B\rho d^3 u_1^2 K_M}$ gyroscopic stability factor

$\bar{s}$ = $\dfrac{2(K_L - k_1^{-2} K_T)}{K_L + k_2^{-2} K_H - k_1^{-2} K_A}$ dynamic stability factor

S_L Radius of lift swerving motion

α_1 Exponential damping coefficient of fast rate

α_2 Exponential damping coefficient of slow rate

δ Magnitude of yaw angle

$\bar{\delta}^2$ Mean yaw squared

ϵ_y Standard error for fit of yaw curve to data

ϵ_s Standard error for fit of swerving motion curve to data

ρ_o Standard sea level air density

ρ Air density

INTRODUCTION

A program of 20mm models with square and hemispherical bases* was fired in Exterior Ballistics Laboratory's small aerodynamic free flight spark range in order to try to determine comparative aerodynamics of these configurations. The results obtained from the 32 rounds which could be reduced are given in this report. The four types of models fired consisted of the basic 5.183 calibers long, square based model and three modifications: (1) the addition of a hemispherical base, (2) the addition of a 0.556 caliber cylinder, and (3) the addition of a 0.556 caliber cylinder plus a hemispherical base. The second modification was made to determine whether the added length of the hemisphere was the cause of instability, and the third modification was made to see if the addition of the hemisphere to the longer model gave the same type of changes as the first modification. All four models can be seen in Figure 1 with the dimensions being given in Figure 2. The customary methods of data reduction(1) were used.

AERODYNAMIC COEFFICIENTS

The drag coefficient as obtained from the least squares fit of a cubic equation in distance down range to the time interval contains the effect of the variation of this coefficient with yaw as shown by

$$K_D = K_{Do} + K_{D_\delta 2}\,\overline{\delta}^{\,2}.$$

Since there were very few rounds which had different yaws at essentially the same Mach number, it was not possible to determine $K_{D_\delta 2}$ by a fit of K_D to $\overline{\delta}^{\,2}$. A value of $K_{D_\delta 2} = 2.0$ per radian squared was therefore assumed in order to determine the values of K_{Do} (see Figure 7). Values of the spin deceleration coefficient, K_A, could not be determined because pins for a spin reduction were not placed in the bases of the models.

*Additional data on hemispherical based shell can be found in Reference 7.

Although there is a variation of K_N with the yaw, the yaw for this set of rounds is so small that the correction has been neglected. The curves for K_N as shown in Figure 8 seem to be quite well defined and show an appreciable difference between the square and hemispherical based models which is not attributable to experimental inaccuracy. It was felt that the values of K_N for corresponding bases were within the accuracy of determination, therefore only one curve for each type of base was drawn. There is not enough data in the transonic region to accurately determine the shape of the K_N or the K_M curve in the neighborhood of M = 1. The general trend of the curves of K_N and K_M vs. Mach number have, therefore, been drawn to agree with Reference 2. Since the overturning moment coefficient is contaminated by the different c.m. locations for the different models, the values of K_M for the square based models have been evaluated at a point which is the same distance from the nose of the c.m. of the hemispherical based model of comparable length and are denoted K_M^* (see Figure 9). The plot of the center of pressure of the normal force shown in Figure 10, together with K_N, are probably even more descriptive of the effect of the hemispherical base on the overturning moment than the plot of K_M.

The curves of the Magnus moment in Figure 11 are some of the better determined curves obtained from this firing. Again there is a distinct difference in the values of the hemispherical and square based models especially in the range of $M > 1.1$. Again it was felt that only one curve for each base type was warranted. Since the swerve due to the Magnus force for all of these rounds, was less than the accuracy of measurement the determination of K_F with any degree of accuracy was impossible.

The damping moment coefficients in Figure 12 also show only a trend, but they do indicate a distinct difference in the two types of bases which is not attributable to experimental error. Values of the damping force could not be obtained since models of the same configuration but with different center of mass location were not fired.

The values of the coefficients near Mach = 1 may be affected by the interference of reflected nose shock waves with the afterbody of the model, therefore there is some doubt as to their accuracy.

DISCUSSION

The outstanding difference in the shadowgraphs of the square and hemispherical based models is the flow over part of the hemisphere and the resulting shock wave when the boundary layer separates from the base, as is shown in Figures 3 and 4.

There is a very distinct difference in the drag coefficients of the square and hemispherical based models, with the hemispherical base displaying a noticeably greater drag than the square based models (see Figure 7). The drag for a short, large angled boattail is higher than that for a square based missile as is shown in Reference 4 and is theoretically discussed by J. Sternberg[5]. The separation of the flow from the hemispherical base in essence gives a short, large angled boattail.

The normal force is increased by the addition of a hemispherical base to the rear of a regular square base. The largest difference in K_N for the two types of bases is in the transonic region. Since the center of pressure of the normal force is moved rearward by the addition of the hemispherical base as seen in Figure 10, it seems that there has been an increase in the pressure difference at the rear of the projectile. This pressure difference could be the result of the difference in separation points of the boundary layer on opposite sides of the hemispherical base and the resulting shock wave. The separation angles, which are defined as the angles made by the radius vector from the center of the sphere to the point of separation and the model's axis as illustrated in Figures 5 and 6, were measured on numerous plates. Only in a very few cases measurable differences in the separation angles on the two sides of the projectile were obtained.

Two photographs illustrating a large difference in separation angles are shown in Figures 5 and 6 where a difference of 3° and 2° respectively, was measured.

The largest difference in the normal forces and their centers of pressure as well as in the overturning moments is in the transonic region with the difference decreasing for increasing Mach number. This indicates that there are changes in the flow forward of the base due to the additional shock wave at the point of the boundary layer separation from the hemispherical base. This disturbance could be propagated forward in the boundary layer and also in the potential flow at transonic Mach numbers. With the aid of this observation the change in the normal force coefficient due to the addition of a hemispherical base can be checked by means of the change in the overturning moment coefficient and some assumptions about the location of the normal force.

Since the overturning moment coefficients for the square based models have been evaluated at the position of the c.m. of the corresponding hemispherical based models, the difference in the coefficients should be completely due to the change in the flow caused by the addition of the boattail. Munk's linearized slender body theory predicts a change in the normal force on a projectile corresponding to the change in its cross sectional area. Therefore, it seems reasonable to assume that the coefficient, ΔK_N, which represents the change in normal force coefficient due to the addition of the hemisphere will act at a point in the region in which the projectile is undergoing the decrease in cross sectional area. The effective boattail is from the beginning of the hemisphere to the separation point, and is about 0.10 calibers in length. It will be assumed that ΔK_N acts at the middle of this region. For the short hemispherical based model, where the beginning of the hemisphere is 1.65 calibers behind the c.m., the distance from the c.m. to ΔK_N is

$$C.P._{\Delta K_N} = 1.70 \pm 0.2 \text{ calibers},$$

and for the long hemispherical based model, where the beginning of the hemisphere is 1.92 calibers behind the c.m.

$$C.P._{\Delta K_N} = 1.97 \pm 0.2 \text{ calibers},$$

where the $\pm$ 0.2 caliber is used to give a probable limit to the value.

If the value of the change in K_M between the square and hemispherical based models of corresponding lengths is obtained from the graph in the appendix and it is assumed that

$$\hat{K}_M - K_M^* = (C.P._{\Delta K_N})\Delta K_N,$$

where $\hat{K}_M$ is the moment coefficient for the hemispherical based model, then ΔK_N can be computed. Using this ΔK_N and $\hat{K}_N = K_N + \Delta K_N$, the following table shows a comparison of predicted and observed values of $\hat{K}_N$.

Model Type*	Mach Number	Calculated ΔK_N	Calculated K_N	Observed K_N
SH	0.9	0.18 $\pm$ 0.02	1.11 $\pm$ 0.02	1.12
LH	0.9	0.18 $\pm$ 0.02	1.11 $\pm$ 0.02	1.12
SH	1.6	-0.006 $\pm$ 0.001	1.014 $\pm$ 0.001	1.10
LH	1.6	0.000	1.02	1.10

These show good agreement with the observed values, especially at M = 0.9.

The damping moment coefficient for the hemispherical based models is markedly negative in the transonic region and seems to be approaching a zero or positive value as the Mach number increases as shown in Figure 12. Since a positive K_H indicates that there is a resistance to the change in yaw, the negative K_H means that the amount of yaw is being increased. Under these circumstances the projectile is unstable.

On the basis of the good agreement obtained for the estimate of the normal force coefficient, it is felt that a fairly good estimate of K_S can also be obtained in the same manner.

* Model types are identified in Table I of the Appendix.

The damping force is considered to be the same type of phenomenon as the normal force, i.e., caused by the change in the momentum of the potential flow. The velocity field, however, is the result of the velocity induced by the cross spin rather than the cross velocity due to yaw. It therefore seems reasonable to assume that the location of ΔK_S is at the same place as ΔK_N. Although K_S for the square based models is not known, a comparison of the known force coefficients of this report with those in References 2 and 3 indicate that the forces for the two slightly different models are about the same within about 5%.

Therefore, using References 2 and 3, it is assumed that $K_S = -6.0$ for the short and long square based models at M = 0.9. At M = 1.6 this value is - 4.0. These K_S values and the square based model K_H values of this report, which are at the c.m. of the square based models, are evaluated at a point corresponding to the c.m. of the hemispherical based models and listed in the following table.

Model Type	Mach Number	K_S^*	K_H^*
SS and LS	0.9	- 5.8	- 2.6
SS and LS	1.6	- 3.8	4.2

Similar to the previous discussion it is assumed that:

$$\hat{K}_H - K_H^* = (C.P._{\Delta K_S})\Delta K_S$$

and

$$\hat{K}_S = K_S^* + \Delta K_S.$$

The following table gives computed values of $\hat{K}_S$.

Model Type	Mach Number	Calculated ΔK_S	Calculated K_S
SH and LH	0.9	2.5 ± 0.5	-3.3 ± 0.5
SH and LH	1.6	3.1 ± 0.6	-0.7 ± 0.6

These estimates indicate that the change in damping force in a positive direction is quite pronounced.

Figure 11 shows that the addition of the hemispherical base causes the Magnus moment to assume a large positive value even in the supersonic region. This condition alone is sufficient for instability.

In Reference 6 it can be seen that the limits for dynamic stability are

$$(1) \quad K_L + k_2^{-2} K_H - k_1^{-2} K_A > 0,$$

$$(2) \quad 0 < \bar{s} < 2,$$

$$(3) \quad s \geq \frac{1}{\bar{s}(2 - \bar{s})} ,$$

where s is the gyroscopic stability factor and $\bar{s}$ is the dynamic stability factor.*

As shown in Table III of the Appendix, all of the hemispherical based models are gyroscopically stable ($s > 1$). Only two of the models, however, satisfy the dynamic stability condition that $0 < \bar{s} < 2$, and these two models do not satisfy the condition that $s \geq \frac{1}{\bar{s}(2 - \bar{s})}$. It is interesting to note that even if K_H were positive for the hemispherical based models, they would still not be stable because of the large positive Magnus moment. Average values of the coefficients for the hemispherical based models for this report are as follows:

$K_L \approx 1.0$	$\frac{\rho d^3}{m} \approx 0.5$
$K_D \approx 0.15$	$k_1^{-2} \approx 10$
$K_T \approx 0.4$	$k_2^{-2} \approx 0.6$
$K_H \approx -4.0$	$K_A \approx 0.01$

With the aid of the conditions (1) and (2) for dynamic stability, an interesting observation can be made. If $K_H = 4.0$ instead of being negative then

$$K_L + k_2^{-2} K_H - k_1^{-2} K_A \approx 1.0 + 0.6\ (+4.0) - 10(0.01) \approx 3.3$$

*Algebraic definition of $\bar{s}$ is given in the Table of Symbols.

and the first condition is satisfied. The dynamic stability factor

$$\bar{s} = \frac{2(K_L - k_1^{-2} K_T)}{K_L + k_2^{-2} K_H - k_1^{-2} K_A} \approx \frac{2\ [1.0 - 10(0.4)]}{3.3} = -1.8$$

and the missile would still be unstable, since $\bar{s}$ is not between 0 and 2.

A further examination of the Magnus effects shows an interesting feature about them. The Magnus effects are usually thought to be a boundary layer phenomenon. Since the effects of the additional shock wave on the hemispherical base would be felt upstream in the subsonic boundary layer and result in a change in the boundary layer characteristics, it is conceivable that there would be changes in the Magnus force and moment. The change in the Magnus moment is verified by Figure 11.

The Magnus force coefficient is also estimated by the same procedure as was used for K_N and K_S; however, the point of application of the force ΔK_F is assumed to be different than that for the other two forces. The relatively large rotating band is believed to be a natural boundary; therefore, the effect of the additional shock wave is assumed to influence the boundary layer flow only behind the rotating band. If ΔK_F is assumed to act at the center of the region between the rear of the rotating band and the point of boundary layer separation then,

$$C.P._{\Delta K_F} = 1.40 \pm 0.2 \text{ calibers}$$

for the short hemispherical based model and

$$C.P._{\Delta K_F} = 1.40 \pm 0.4 \text{ calibers}$$

for the long hemispherical based model. The tolerance allows the force to have limits covering almost the whole effected region. Again using References 2 and 3 it is assumed that $K_F = 0.08$ and 0.15 for $M = 0.9$ and 1.6 respectively for both the short and long models since there is no effect of length for the length of models used[3]. The graph values of K_T for the square based models are evaluated at a point corresponding to the c.m. of the hemispherical based models to give the following table

Model Type	Mach Number	K_T	K_T^*
SS and LS	0.9	0.39	0.40
SS and LS	1.6	-0.13	-0.10

As before it is assumed that

$$\widehat{K}_T - K_T^* = (C.P._{\Delta K_F})\Delta K_F$$

and

$$\widehat{K}_F = K_F + \Delta K_F$$

It is then found that the estimated values are as shown in the following table

Model Type	Mach Number	ΔK_F	$\widehat{K}_F$
SH and LH	0.9	-0.09 ± 0.02	-0.01 ± 0.02
SH and LH	1.6	-0.36 ± 0.06	-0.21 ± 0.06

The change in K_F seems to be a very outstanding indication of the affect of the hemispherical base since it changes from a positive quantity for the square based models to a negative quantity for the hemispherical based models. This change is very pronounced at M = 1.6.

ACKNOWLEDGEMENT

The formulation of this program and the data reduction were directed by B. G. Karpov. The author also wishes to express his appreciation for the contributions of C. H. Murphy to the analysis of the data and the determination of an estimate for the Magnus and damping forces.

Ralph E. Deitrick

RALPH E. DEITRICK

REFERENCES

(1) Murphy, C.H., Data Reduction for the Free Flight Spark Ranges, BRL Report 900 (1954).

(2) Schmidt, L.E., Murphy, C.H., The Aerodynamic Properties of the 7-Caliber Army-Navy Spinner Rocket in Transonic Flight, BRLM Report 775 (1954).

(3) Murphy, C.H., Schmidt, L.E., The Effect of Length on the Aerodynamic Characteristics of Bodies of Revolution in Supersonic Flight, BRL Report 876 (1953).

(4) Karpov, B.G., Renard, Elliot, Effect of Boattailing on Aerodynamic Characteristics of 7-Caliber Long Body of Revolution at M = 1.70, (To be published).

(5) Sternberg, J., Effect of Boattailing on the Base Pressure, Memorandum to R.H. Kent (1948).

(6) Murphy, C.H., On Stability Criteria of the Kelly-McShane Linearized Theory of Yawing Motion, BRL Report 853 (1953).

(7) Roschke, E. J., The Drag and Stability Properties of the Hemispherical Base Shell, 75mm, T50E2, BRL Memorandum Report No. 927 (1955).

APPENDIX

Table I - Physical dimensions

Table II - Aerodynamic Coefficients

Table III - Yaw and swerve characteristics

Figure 1 - Photograph of models

Figure 2 - Drawing of model

Figure 3 - Shock wave comparison, M = 0.93

Figure 4 - Shock wave comparison, M = 1.65

Figure 5 - Separation angle difference

Figure 6 - Separation angle difference

Figure 7 - K_{D_o} vs. M

Figure 8 - K_N vs. M

Figure 9 - K_M vs. M

Figure 10 - $C.P._N$ vs. M

Figure 11 - K_T vs. M

Figure 12 - K_H vs. M

TABLE I

PHYSICAL DIMENSIONS

Type of Round	Type of Base	Length (calibers)	C.M. from nose (calibers)	$\frac{10^4 m}{\rho_o d^3}$	k_1^{-2} (sq. cal.)	k_2^{-2} (sq. cal.)
SS	Short, square	5.184	3.352	1.869	9.311	0.7042
SH	Short, hemispherical	5.683	3.531	2.049	9.360	0.6138
LS	Long, square	5.740	3.644	2.169	9.094	0.5654
LH	Long, hemispherical	6.240	3.823	2.347	9.154	0.4990

Radius of hemisphere = 0.5 caliber
Diameter of Missiles = 0.786 inches
ρ_o = 0.001225 gm^5/cm^3 (ICAO standard)

TABLE II

AERODYNAMIC COEFFICIENTS

Round	M	$\bar{\delta}^2$	K_D	K_{D_o}	K_L	K_N	K_M	K_M^*	C.P.$_N$	K_T	K_H
3430-SS	0.892	2.8	.0911	.0894	.826	.917	1.168	1.332	2.078	.390	- 2.04
3431-SS	0.898	3.7	.0936	.0914	.842	.936	1.158	1.323	2.114	.293	- 0.89
3429-SS	0.932	0.7	.0940	.0936	.874	.968					
3422-SS	1.028	0.7	.1535	.1531	.740	.894	1.156	1.316	2.058	.054	2.46
3376-SS	1.062	2.3	.1537	.1523	.784	.938	1.146	1.314	2.130	- .081	5.16
3454-SS	1.637	2.0	.1285	.1273	.921	1.050	1.072	1.260	2.331	- .146	4.29
3453-SS	1.693	1.05	.1241	.1235	.928	1.052	1.066	1.254	2.339	- .071	1.41
3433-SH	0.911	4.16	.1011	.0986	1.033	1.134	1.036		2.618	.590	- 9.61
3434-SH	0.911	6.86	.1068	.1026	.992	1.099	1.032		2.592	.464	- 5.57
3432-SH	0.916	6.63	.1064	.1024	1.107	1.213	1.043		2.671	.549	- 6.01
3374-SH	1.101	11.36	.1808	.1739	.971	1.152	1.162		2.522	.501	- 3.72
3372-SH	1.107	11.63	.1808	.1737	.936	1.117	1.178		2.476	.449	- 4.31
3373-SH	1.113	10.39	.1766	.1703	.937	1.114	1.157		2.492	.492	- 6.26
3451-SH	1.650	6.71	.1364	.1323	.957	1.093	1.270		2.369	.326	- 1.35
3452-SH	1.671	5.74	.1325	.1290	.990	1.123	1.282		2.389	.360	- 1.10
3436-LS	0.925	1.22	.0962	.0955	.857	.953					
3455-LS	0.930	2.70	.0984	.0968	.853	.951	1.358	1.528	2.217	.365	- .21
3437-LS	0.933	4.13	.1018	.0993	.833	.935	1.362	1.529	2.187	.318	- 1.68
3424-LS	1.011	1.37	.1513	.1505	.833	.984	1.386	1.562	2.236	.106	3.53
3425-LS	1.035	1.27	.1553	.1545	.803	.958	1.400	1.571	2.183	- .012	5.30
3423-LS	1.077	0.69	.1515	.1511	.841	.993	1.383	1.561	2.251	- .090	6.60
3445-LS	1.620	1.20	.1304	.1297	.866	.996	1.398	1.576	2.241	- .167	4.73
3444-LS	1.629	0.26	.1270	.1268							
3446-LS	1.655	2.29	.1300	.1286	.900	1.030	1.399	1.583	2.286	- .123	3.87
3440-LH	0.992	5.35	.1158	.1126	1.036	1.152	1.160		2.816	.479	- 1.81
3439-LH	0.926	3.80	.1164	.1141	1.038	1.154	1.223		2.764	.527	- 8.85
3427-LH	1.024	7.19	.1830	.1786	.993	1.176					
3426-LH	1.035	24.39	.1952	.1804	.900	1.095	1.388		2.556	.433	- 4.83
3428-LH	1.047	27.11	.1981	.1816	.900	1.098	1.390		2.557	.469	- 7.23
3449-LH	1.605	7.19	.1416	.1372	.899	1.041	1.564		2.320	.528	-10.36
3450-LH	1.615	8.56	.1402	.1350	.886	1.026	1.585		2.278	.415	- 6.81
3447-LH	1.624	4.83	.1382	.1353	.992	1.130	1.594		2.413	.447	2.13

TABLE III

YAW AND SWERVE CHARACTERISTICS

Round	$\lvert K_1 \rvert$	$\lvert K_2 \rvert$	$10\bar{\alpha}_1^2$	$10\bar{\alpha}_2^2$	ϵ_Y	S_L	ϵ_S	s	$\bar{s}$	$\frac{\rho}{\rho_o}$
3430-SS	.0071	.0268	.254	- .305	.0012	.140	.0111	2.03	8.42	.9874
3431-SS	.0103	.0312	.230	- .215	.0012	.164	.0117	2.03	-23.46	.9851
3429-SS	.0025	.0129		- .451	.0016	.073	.0092			.9901
3422-SS	.0096	.0108	.210	- .008	.0010	.053	.0099	2.05	.20	.9872
3376-SS	.0159	.0201	.246	.105	.0013	.100	.0069	2.11	.70	.9684
3454-SS	.0179	.0167	.121	.194	.0013	.110	.0081	2.21	1.17	.9780
3453-SS	.0106	.0152	.006	.147	.0010	.094	.0072	2.23	1.70	.9749
3433-SH	.0066	.0319	.024	- .382	.0019	.281	.0222	2.13	1.82	.9819
3434-SH	.0134	.0412	.122	- .299	.0019	.351	.0183	2.15	2.70	.9788
3432-SH	.0097	.0402	.180	- .370	.0032	.348	.0586	2.10	3.06	.9848
3374-SH	.0108	.0537	.262	- .350	.0039	.356	.0455	1.97	5.43	.9518
3372-SH	.0149	.0545	.189	- .307	.0030	.324	.0248	1.92	3.70	.9658
3373-SH	.0129	.0514	.124	- .328	.0032	.324	.0440	1.93	2.48	.9666
3451-SH	.0160	.0407	.237	- .224	.0019	.211	.090	1.83	-55.00	.9771
3452-SH	.0127	.0380	.286	- .261	.0019	.204	.0179	1.81	-18.25	.9758
3436-LS	.0026	.0164		- .496	.0016	.075	.0089			.9790
3435-LS	.0106	.0251	.329	- .278	.0010	.104	.0055	1.69	- 7.27	.9802
3437-LS	.0169	.0300	.209	- .216	.0011	.120	.0061	1.70	24.40	.9790
3424-LS	.0108	.0170	.272	- .067	.0014	.062	.0095	1.65	- .10	.9929
3425-LS	.0112	.0158	.244	.029	.0011	.058	.0084	1.64	.49	.9915
3423-LS	.0087	.0112	.230	.096	.0010	.052	.0074	1.64	.74	.9907
3445-LS	.0133	.0134	.053	.192	.0010	.052	.0078	1.67	1.37	.9667
3444-LS	.0077	.0042			.0009	.018				.9763
3446-LS	.0173	.0200	.053	.164	.0012	.078	.0096	1.65	1.33	.9801
3440-LH	.0086	.0370	.320	- .310	.0018	.285	.0180	1.88	-85.04	.9767
3439-LH	.0106	.0305	.092	- .302	.0022	.202	.0197	1.78	2.21	.9667
3427-LH	.0024	.0383		- .585	.0031	.262	.0237			.9883
3426-LH	.0233	.0788	.206	- .290	.0020	.325	.0189	1.54	3.91	.9896
3428-LH	.0213	.0834	.138	- .299	.0035	.352	.0180	1.54	2.46	.9934
3449-LH	.0055	.0424	.081	- .344	.0025	.143	.0264	1.40	1.82	.9809
3450-LH	.0133	.0471	.117	- .267	.0019	.145	.0180	1.41	2.26	.9770
3447-LH	.0099	.0347	.547	- .408	.0017	.125	.0132	1.41	- 3.09	.9736

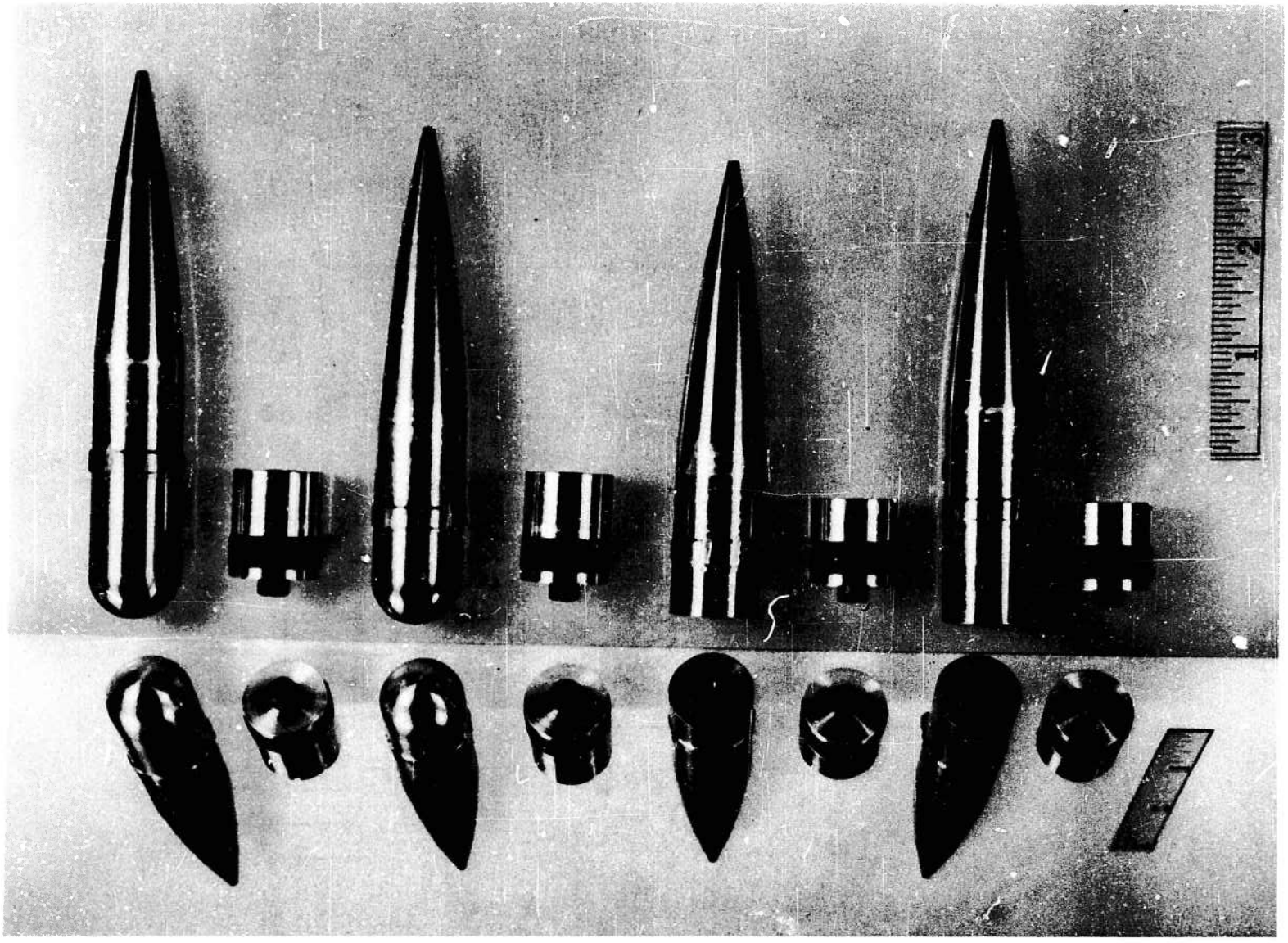

FIGURE 1

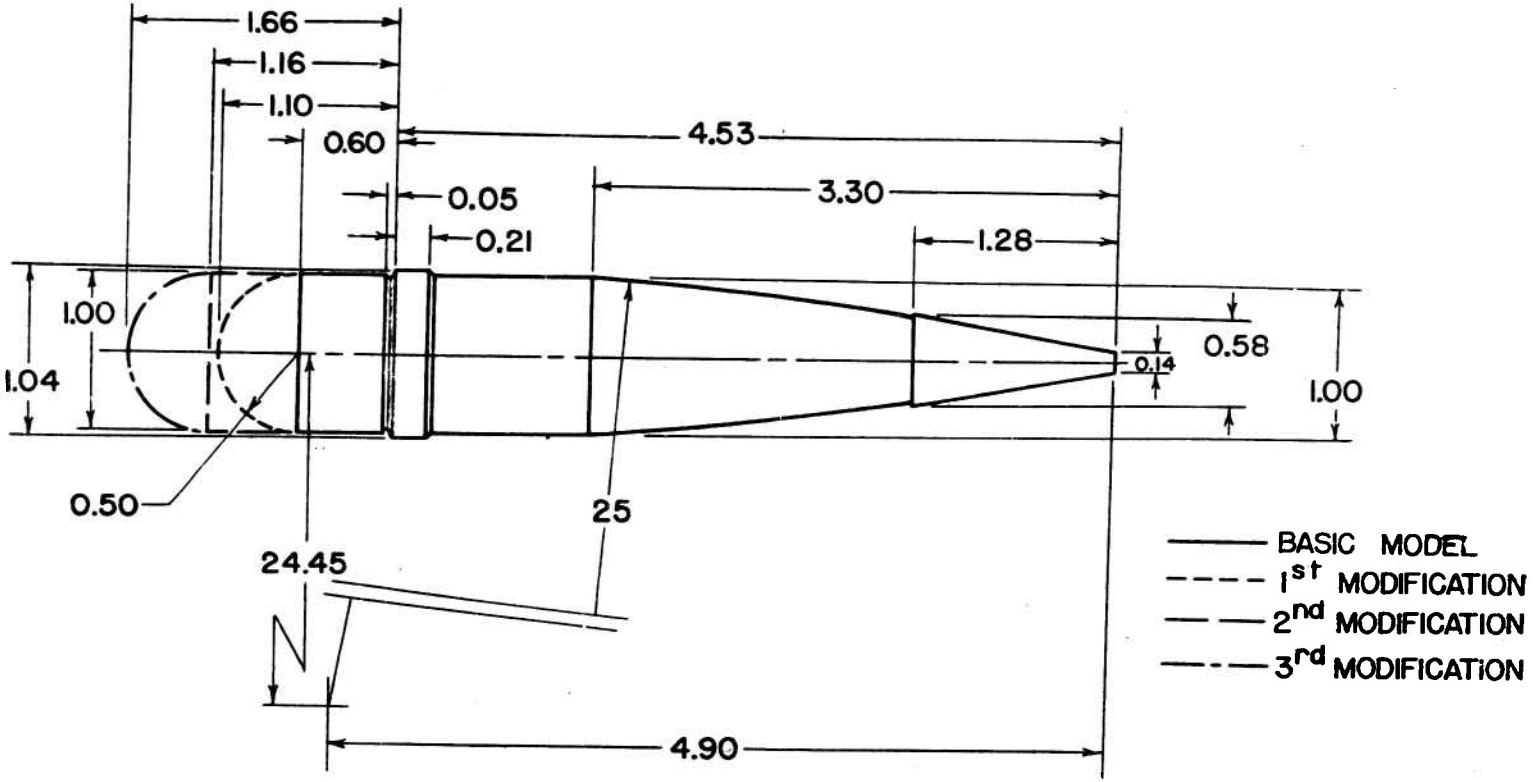

ALL DIMENSIONS IN CALIBERS

FIGURE 2

Rd. 3435-SS M = .93

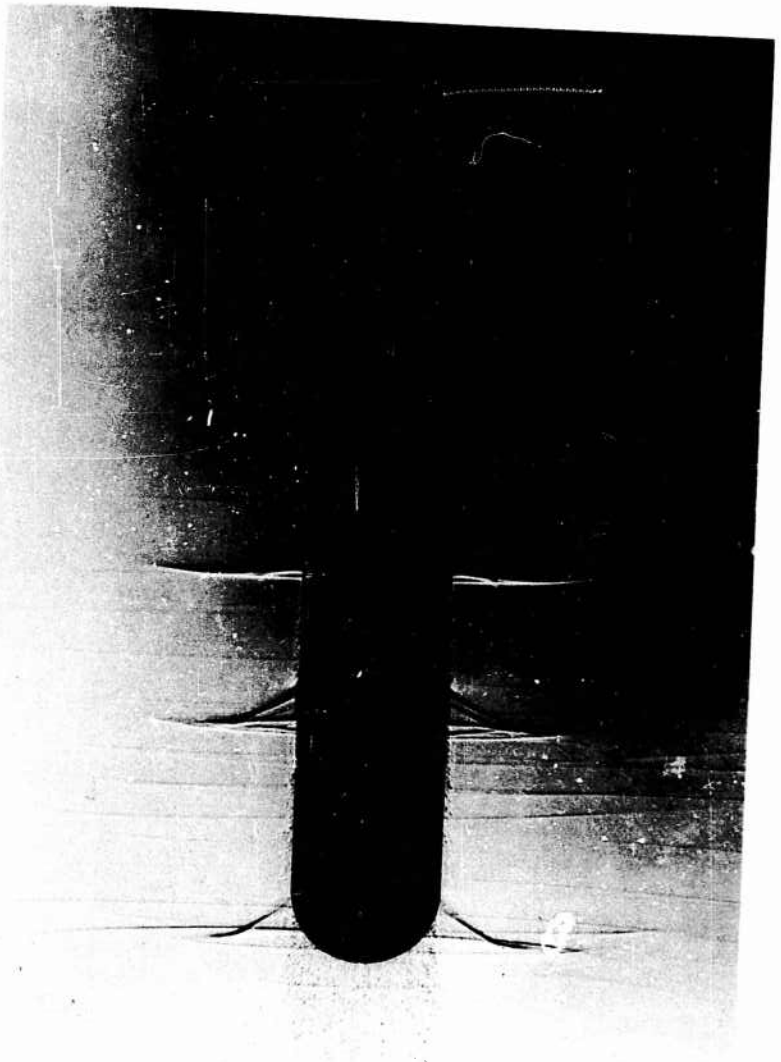

Rd. 3439-SH M = .93

FIG. 3.

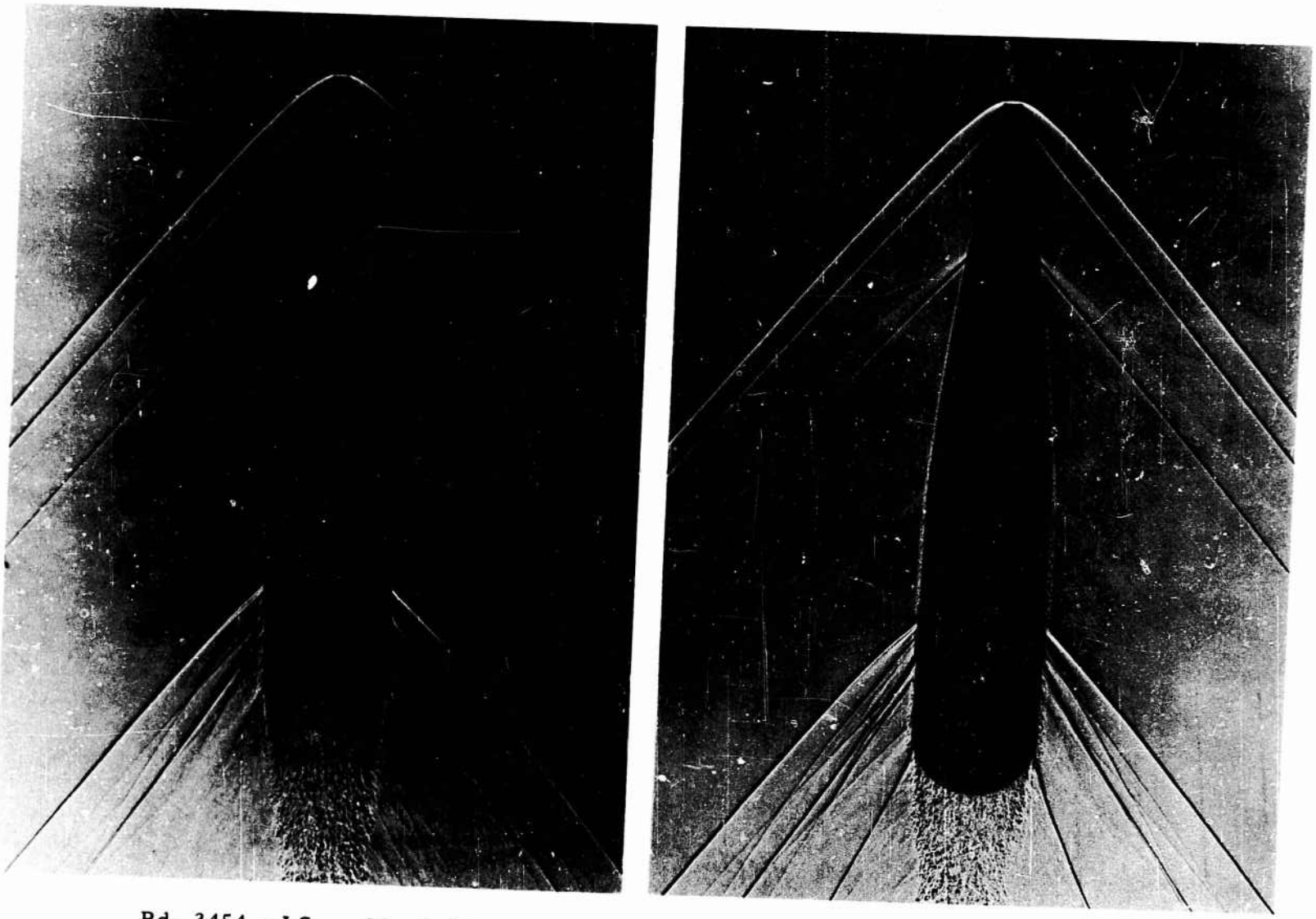

Rd. 3454 - LS M = 1.64

Rd. 3451 - LH M = 1.65

FIG. 4.

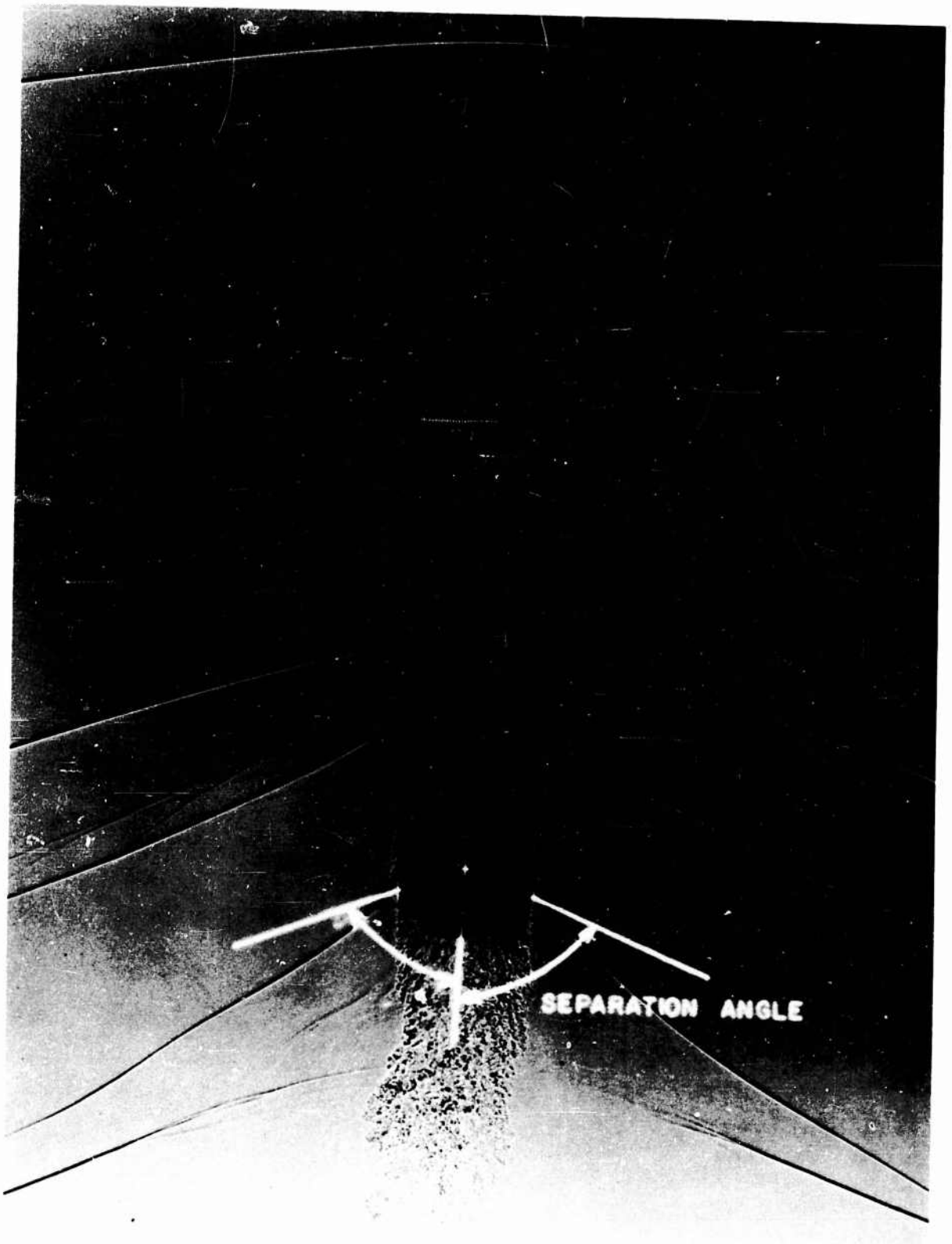

FIG. 5. Separation angle difference - 3°
Rd. 3426-LH M = 1.035

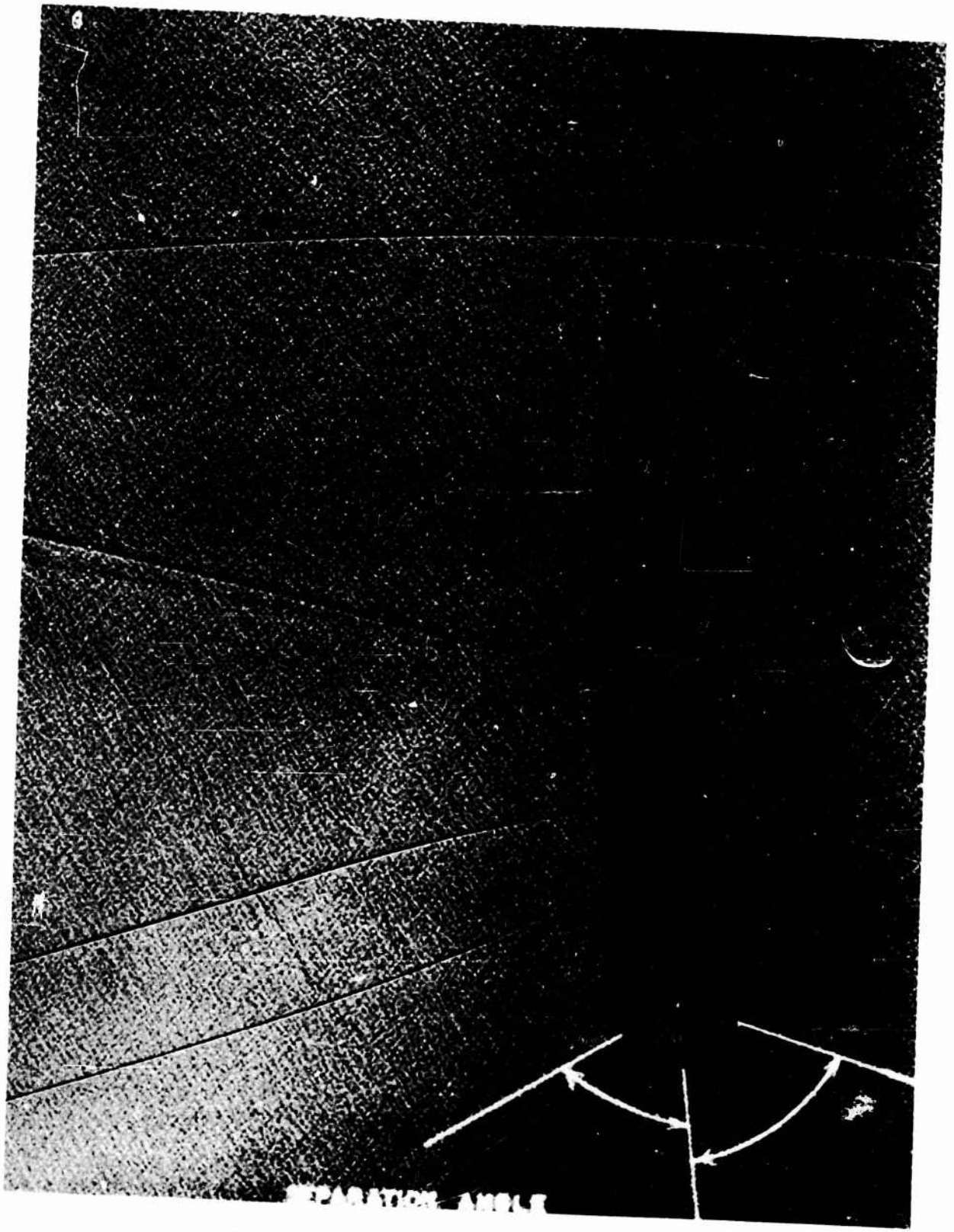

FIG. 6. Separation angle difference = 2°
Rd. 3426-LH M = 1.047

ARMY - OS - ABERDEEN PROVING GROUND MD

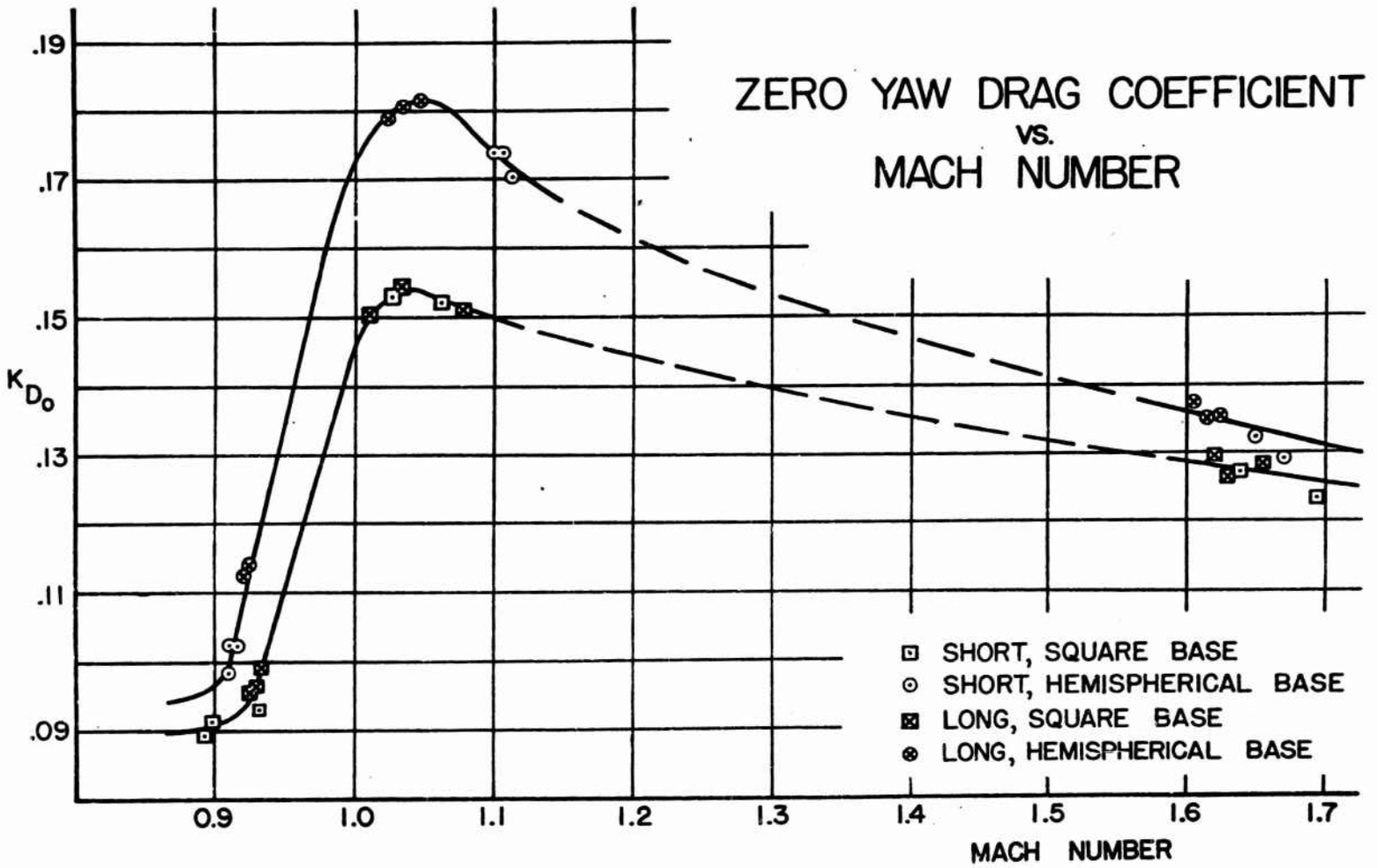
ZERO YAW DRAG COEFFICIENT
VS.
MACH NUMBER
.19
.17
.15
.13
.11
.09
K_{D_o}
0.9
1.0
1.1
1.2
1.3
1.4
1.5
1.6
1.7
MACH NUMBER
SHORT, SQUARE BASE
SHORT, HEMISPHERICAL BASE
LONG, SQUARE BASE
LONG, HEMISPHERICAL BASE

FIGURE 7

NORMAL FORCE COEFFICIENT
vs.
MACH NUMBER

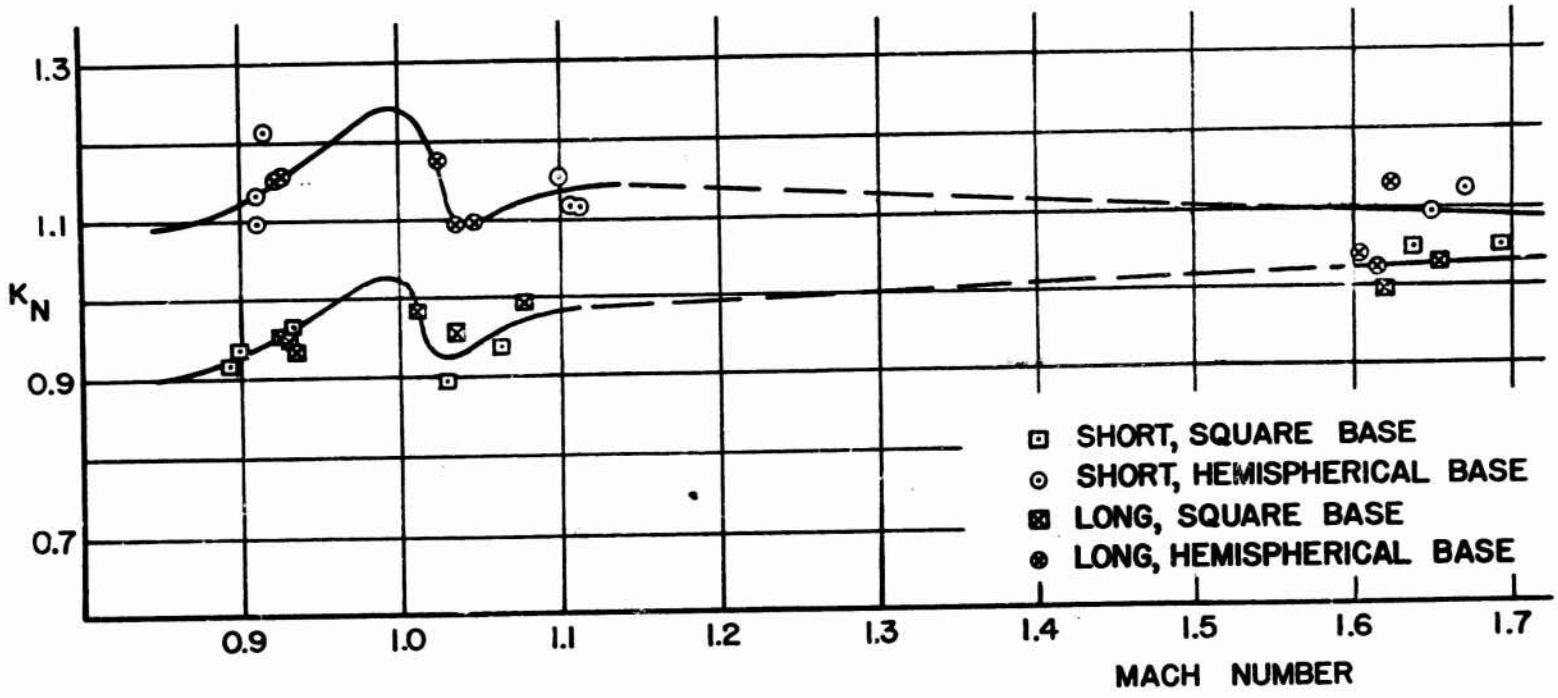

FIGURE 8

OVERTURNING MOMENT COEFFICIENT
vs.
MACH NUMBER

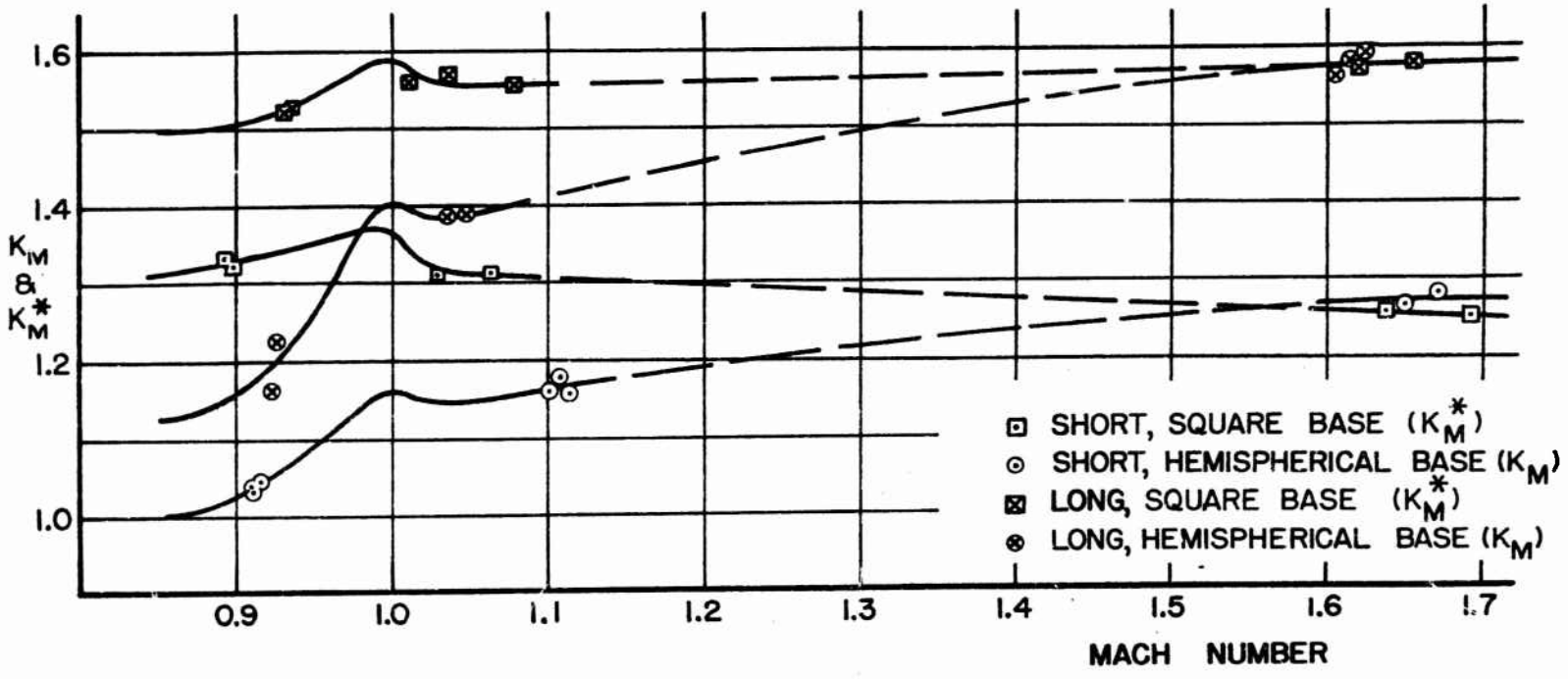

FIGURE 9

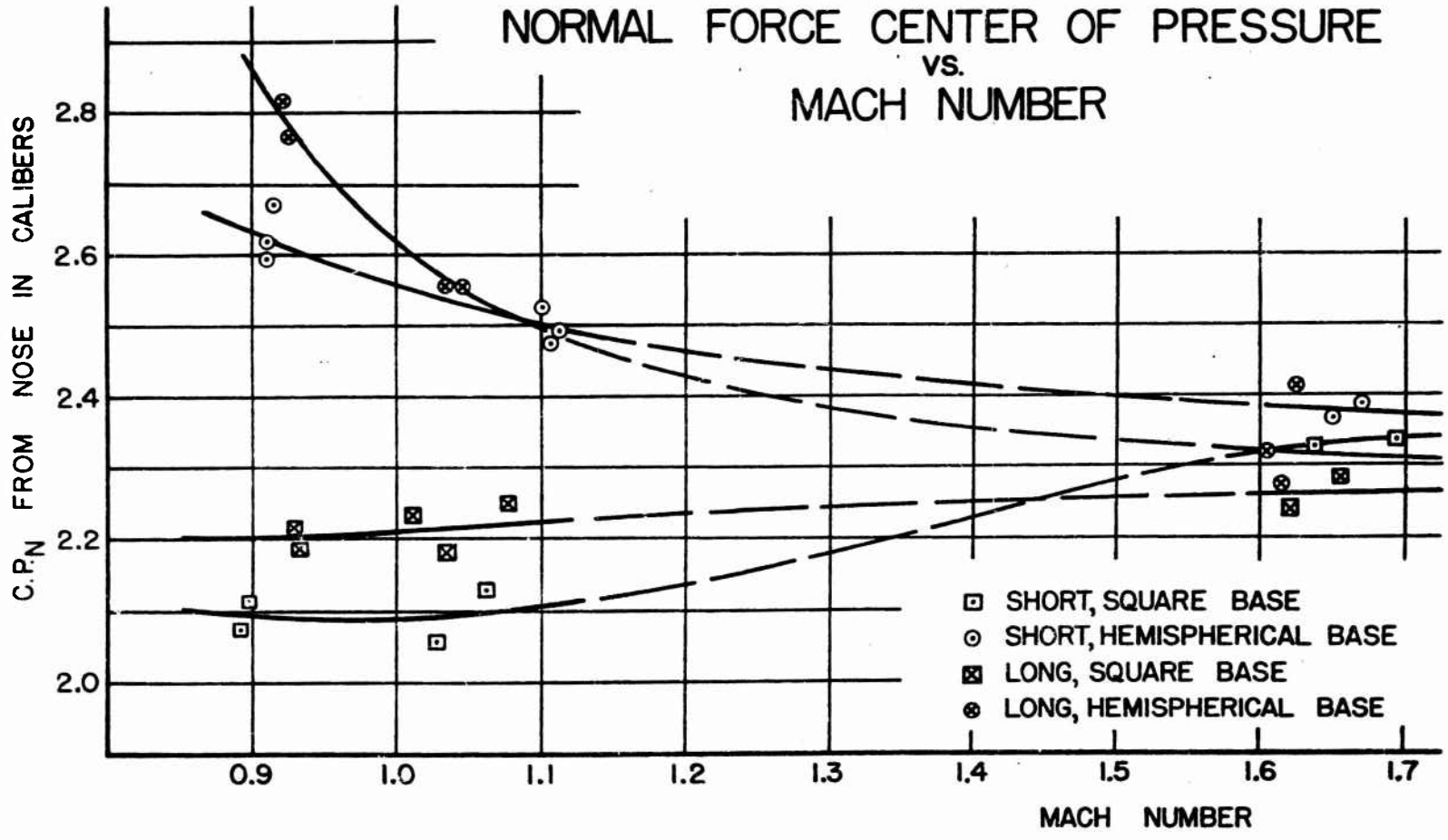
NORMAL FORCE CENTER OF PRESSURE
vs.
MACH NUMBER
C.P.N FROM NOSE IN CALIBERS
2.8
2.6
2.4
2.2
2.0
0.9
1.0
1.1
1.2
1.3
1.4
1.5
1.6
1.7
MACH NUMBER
SHORT, SQUARE BASE
SHORT, HEMISPHERICAL BASE
LONG, SQUARE BASE
LONG, HEMISPHERICAL BASE

FIGURE 10

MAGNUS MOMENT COEFFICIENT vs. MACH NUMBER

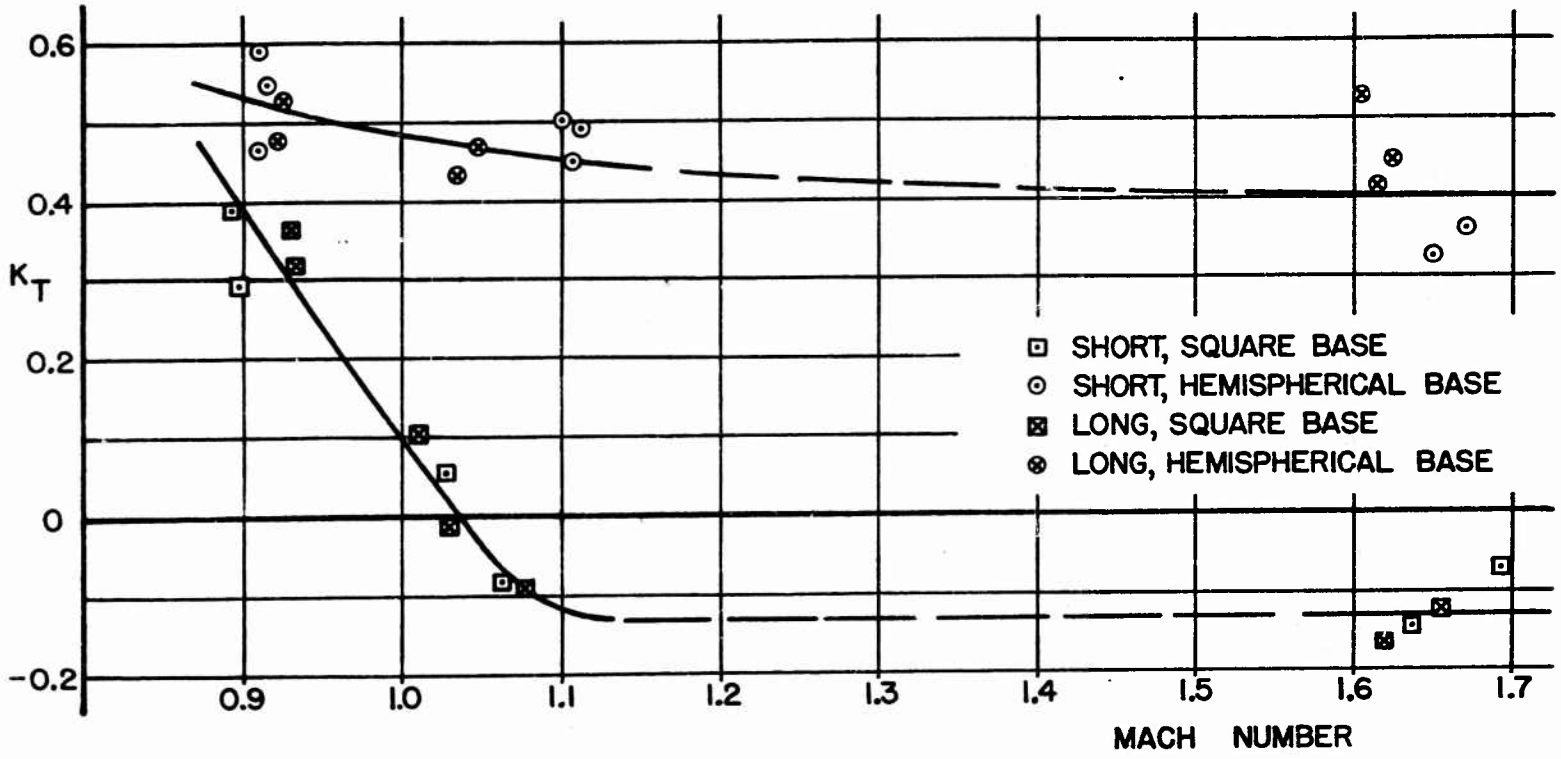

FIGURE 11

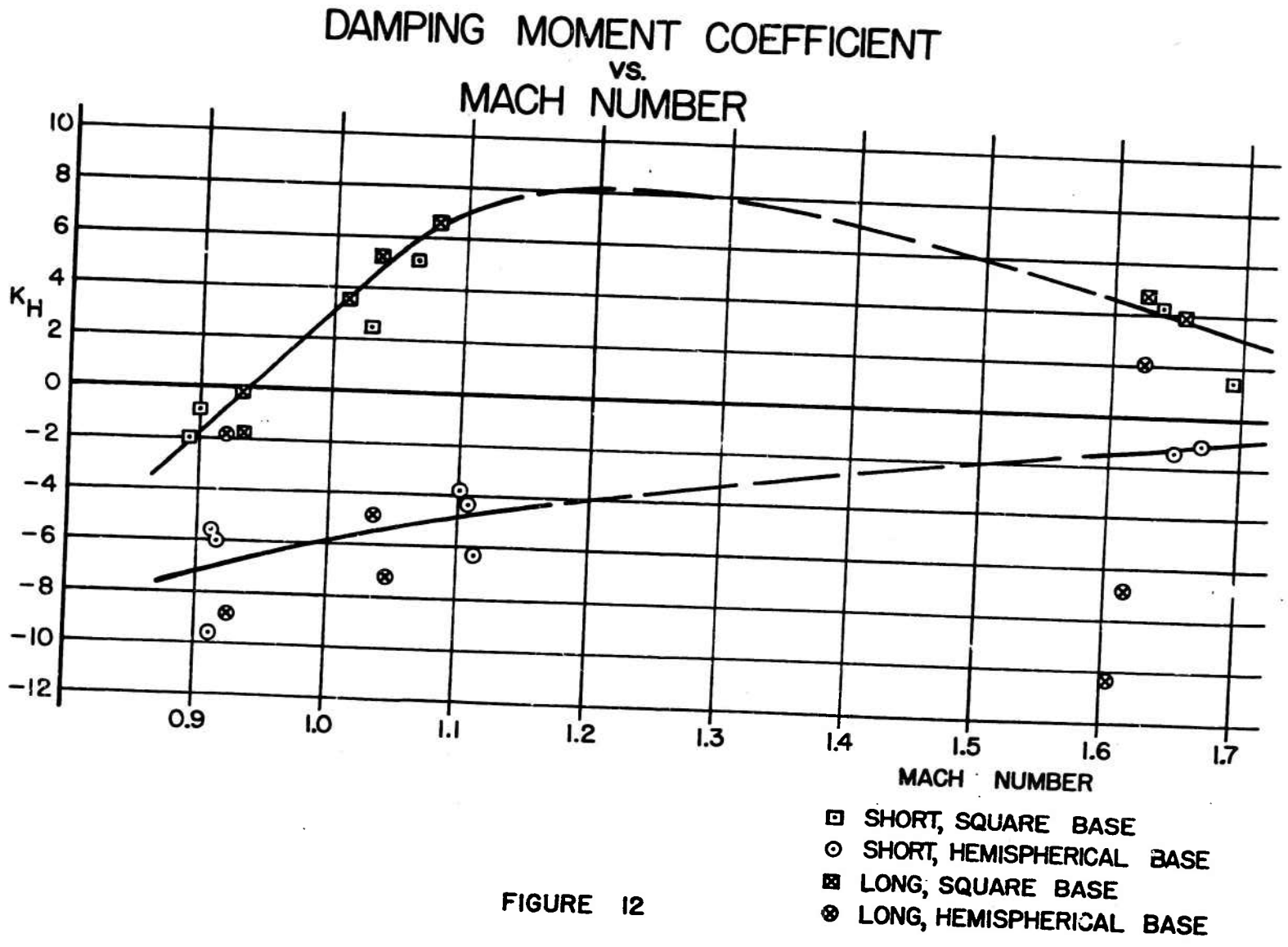
DAMPING MOMENT COEFFICIENT
vs.
MACH NUMBER
K_H
10
8
6
4
2
0
-2
-4
-6
-8
-10
-12
0.9
1.0
1.1
1.2
1.3
1.4
1.5
1.6
1.7
MACH NUMBER
SHORT, SQUARE BASE
SHORT, HEMISPHERICAL BASE
LONG, SQUARE BASE
LONG, HEMISPHERICAL BASE

FIGURE 12

DISTRIBUTION LIST

No. of Copies	Organization
	Chief of Ordnance Department of the Army Washington 25, D. C. Attn: ORDTB - Bal Sec ORDTA ORDTX-AR
10	British Joint Services Mission 1800 K Street, N. W. Washington 6, D. C. Attn: Mr. John Izzard, Reports Officer
4	Canadian Army Staff 2450 Massachusetts Avenue Washington 8, D. C.
3	Chief, Bureau of Ordnance Department of the Navy Washington 25, D. C. Attn: Re3
2	Commander Naval Proving Ground Dahlgren, Virginia
2	Commander Naval Ordnance Laboratory White Oak Silver Spring, Maryland Attn: Mr. Nestingen Dr. May
1	Superintendent Naval Postgraduate School Monterey, California
2	Commander Naval Air Missile Test Center Point Mugu, California

No. of Copies	Organization
1	Commanding Officer U. S. Naval Air Rocket Test Station Lake Denmark, New Jersey
1	Commanding Officer and Director David W. Taylor Model Basin Washington 7, D. C. Attn: Aerodynamics Lab.
1	Commander Naval Air Development Center Johnsville, Pennsylvania
2	Commander Naval Ordnance Test Station China Lake, California Attn: Technical Library
1	Commander Arnold Engineering Development Center Tullahoma, Tennessee Attn: Deputy Chief of Staff, R&D
4	Commander Air Research and Development Command P. O. Box 1395 Baltimore 3, Maryland Attn: Deputy for Development
5	Director Armed Services Technical Information Agency Documents Service Center Knott Building Dayton 2, Ohio Attn: DSC - SA

DISTRIBUTION LIST

No. of Copies	Organization
3	Director National Advisory Committee for Aeronautics 1512 H Street, N. W. Washington 25, D. C.
2	Director National Advisory Committee for Aeronautics Ames Laboratory Moffett Field, California Attn: Dr. A. C. Charters Mr. H. J. Allen
3	National Advisory Committee for Aeronautics Langley Memorial Aeronautical Laboratory Langley Field, Virginia Attn: Mr. J. Bird, Mr. C. E. Brown Dr. Adolf Busemann
1	National Advisory Committee for Aeronautics Lewis Flight Propulsion Lab. Cleveland Airport Cleveland, Ohio Attn: F. K. Moore
2	U. S. Atomic Energy Commission Sandia Corporation P. O. Box 5800 Alburquerque, New Mexico Attn: Mr. Wynne K. Cox
1	Commanding General Redstone Arsenal Huntsville, Alabama Attn: Technical Library
3	Commanding Officer Picatinny Arsenal Dover, New Jersey Attn: Samuel Feltman Ammunition Labs.
1	Commanding Officer Frankford Arsenal Philadelphia, Pennsylvania Attn: Reports Group
1	Commanding Officer Chemical Corps Chemical and Radiological Laboratory Army Chemical Center, Md.
2	Director, JPL Ord Corps Installation 4800 Oak Grove Drive Department of the Army Pasadena, California Attn: Mr. Irl E. Newlan Reports Group
6	Commanding General Ordnance Ammunition Center Joliet, Illinois
1	Operations Research Office 7100 Connecticut Avenue Chevy Chase, Maryland Washington 25, D. C.
2	Applied Physics Laboratory 8621 Georgia Avenue Silver Spring, Maryland Attn: Mr. George L. Seielstad
1	Aerophysics Development Corp. P. O. Box 657, Pacific Palisades, California Attn: Dr. William Bollay
2	Armour Research Foundation Illinois Institute of Technology 35 W. 33rd Street Chicago 16, Illinois Attn: Mr. W. Casier Dr. A. Wundheiler

DISTRIBUTION LIST

No. of Copies	Organization
1	Cornell Aeronautical Lab., Inc. 4455 Genesee Street Buffalo, New York Attn: Miss Elma T. Evans Librarian
1	California Institute of Technology Guggenheim Aeronautical Lab. Pasadena, California Attn: Prof. H. W. Leipman
1	Consolidated Vultee Aircraft Corp. Ordnance Aerophysics Laboratory Daingerfield, Texas Attn: Mr. J. E. Arnold
1	California Institute of Technology Norman Bridge Laboratory of Physics Pasadena, California Attn: Dr. Leverett Davis, Jr.
1	M. W. Kellogg Company Foot of Danforth Avenue Jersey City 3, New Jersey Attn: Mr. Robert A. Miller
1	University of So. California Engineering Center Los Angeles 7, California Attn: Mr. H. R. Saffell Director
1	United Aircraft Corp. Research Department East Hartford 8, Connecticut Attn: Mr. Robert C. Sale
1	University of Michigan Willow Run Research Center Willow Run Airport Ypsilanti, Michigan Attn: Mr. J. E. Corey
1	Wright, Aeronautical Corp. Wood-Ridge, New Jersey Attn: Sales Dept. (Government)
1	Professor George Carrier Division of Applied Sciences Harvard University Cambridge 38, Massachusetts
1	Dr. Clark B. Milliken Guggenheim Aeronautical Lab. California Institute of Technology Pasadena, California
1	Dr. A. E. Puckett Hughes Aircraft Company Florence Avenue at Teal St. Culver City, California
1	Dr. L. H. Thomas Watson Scientific Computing Laboratory 612 West 116th Street New York 27, New York
1	Office Asst. Secretary of Defense (R&D) Committee on Ordnance Washington 25, D. C.